Article

Synthesis and Characterization of Fe–FeO Core–Shell Nanowires and Nanonecklaces

Lirong Lu, Zhihui Ai, Jinpo Li, Zhi Zheng, Quan Li, and Lizhi Zhang

Crystal Growth & Design, **2007**, 7 (2), 459-464 • DOI: 10.1021/cg060633a

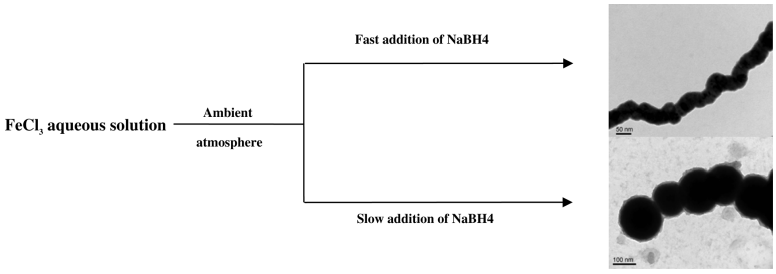

More About This Article

Additional resources and features associated with this article are available within the HTML version:

- Supporting Information
- Links to the 10 articles that cite this article, as of the time of this article download
- Access to high resolution figures
- Links to articles and content related to this article
- Copyright permission to reproduce figures and/or text from this article

View the Full Text HTML

CRYSTAL GROWTH & DESIGN
2007
VOL. 7, NO. 2
459−464

Synthesis and Characterization of Fe−Fe_2O_3 Core−Shell Nanowires and Nanonecklaces

Lirong Lu,[†] Zhihui Ai,[†] Jinpo Li,[†] Zhi Zheng,[‡] Quan Li,[§] and Lizhi Zhang*,[†]

Key Laboratory of Pesticide & Chemical Biology of Ministry of Education, College of Chemistry, Central China Normal University, Wuhan 430079, Institute of Surface Micro and Nano Materials, Xuchang University, Xuchang 461000, and Department of Physics, The Chinese University of Hong Kong, Shatin, New Territories, Hong Kong, People's Republic of China

Received September 21, 2006; Revised Manuscript Received November 21, 2006

ABSTRACT: Fe−Fe_2O_3 core−shell nanowires and nanonecklaces were obtained simply through controlling the reduction rate of Fe^{3+} ions by sodium borohydride in aqueous solution at ambient atmosphere. The resulting materials were characterized by X-ray powder diffraction, scanning electron microscopy images and energy dispersive X-ray spectrum, transmission electron microscopy, elemental mapping, X-ray photoemission spectroscopy, and magnetization measurements. A possible formation mechanism was proposed on the basis of characterization results. It was interesting to find that the core−shell nanowires used in electrochemical-assisted and ultrasound-assisted Fenton-like reaction systems could much more efficiently degrade organic pollutant in aqueous solutions than traditional Fenton reagent Fe^{2+} ions under neutral pH and pH 2, respectively. This study indicates that the resulting iron-containing nanostructures are promising materials in magnetic, environmental, and catalytic fields.

Introduction

Iron-containing core−shell nanostuctured materials have become more and more attractive in recent years, because these materials possess favorable magnetic properties of metallic iron nanoparticles while protecting the nanoparticles from oxidation.[1] Special methods are often required to protect the high active nanosized iron from undesired reactions in order to realize easy and cost-effective applications of these materials. For instance, Dumitrache and co-workers synthesized iron−iron oxide core−shell nanoparticles by laser pyrolysis followed by a superficial oxidation process.[2] In their preparation, harmful iron pentacarbonyl vapors were used. Moreover, it was hard to control the size and shape of the nanoparticles. The method of reducing metal salts by borohydride derivatives has been widely used to synthesize iron-containing nanoparticles in organic solvents.[3,4] Recently, Carpenter and co-workers utilized this reduction method to synthesize iron-containing core−shell nanoparticles in reverse micelles.[5] However, to the best of our knowledge, Fe−Fe_2O_3 core−shell nanowires and nanonecklaces have not been reported so far.

Herein, we report a simple and controllable fabrication of Fe−Fe_2O_3 core−shell nanowires and nanonecklaces for the first time. The synthesis was realized simply through controlling the reduction rate of Fe^{3+} ions by sodium borohydride in aqueous solution at ambient atmosphere. Different from these studies on iron-containing nanoparticles obtained by reducing metal salts by borohydride derivatives,[3−5] our preparation does not involve any organic solvents and therefore is environmentally friendly.

Experimental Section

Synthesis. All chemicals were of analytical grade and were used as received without further purification. In a typical synthesis, 0.15 g of $FeCl_3 \cdot 6H_2O$ was dissolved in 50 mL of deionized water to form a ferric solution (solution 1) and 0.3 g of $NaBH_4$ was added to 20 mL of deionized water to form solution 2. Solution 2 was then dropped into solution 1 at rates of 0.5 and 0.02 mL/s for the synthesis of nanowires and nanonecklaces, respectively. The addition process was preformed at ambient atmosphere without the protection of inert gases or vacuum atmosphere. During the addition, the solutions were shaken by hand (magnetic stirring could not be used in order to avoid magnetically induced aggregation of the resultant iron particles). The solution was bubbled with plenty of gas with the addition of $NaBH_4$ solution, accompanied by fluffy black precipitates that appeared on the surface of the solution. The fluffy black precipitates were washed with deionized water and ethanol and finally dried under nitrogen flow for characterization.

Characterization. X-ray powder diffraction patterns were obtained on a Bruker D8 Advance X-ray diffractometer with Cu Ka radiation ($\lambda = 1.54178$ Å). Scanning electron microscopy (SEM) images and an energy-dispersive X-ray spectrum were performed on a LEO 1450VP scanning electron microscope. Transmission electron microscopy images were recorded on a Tecnai 20 FEG transmission electron microscope with an energy-dispersive X-ray instrument. The elemental mapping was performed using a Gatan image filtering system attached to the same microscope. X-ray photoemission spectroscopy was recorded on a Kratos ASIS-HS X-ray photoelectron spectroscope equipped with a standard and monochromatic source (Al Ka) operated at 150 W (15 kV, 10 mA). The magnetization curves and hysteresis loop of the nanocomposite were characterized with a Lake model 7300 VSM.

Results and Discussion

Figure 1 shows X-ray diffraction (XRD) patterns of the as-prepared samples. All of the peaks of XRD patterns can be readily indexed to body-centered cubic Fe [space group, *Im*3*m* (229)]. The peaks at 44.9 and 65.0° can be indexed to the (110) and (200) planes of cubic Fe (JCPDS, file no. 06-0696, $a = 0.2866$ Å). It was found that the crystal size of Fe decreased with a decrease on the addition rate of $NaBH_4$ solution.

Figure 2 shows SEM images of the as-prepared samples obtained with different addition rates of $NaBH_4$ solution. It was found that wirelike nanostructures were obtained when the addition rate of $NaBH_4$ solution was 0.5 mL/s (Figure 2a). The resulting nanowires are 50−100 nm in diameter and several to several tens of micrometers in length. When the addition rate of the $NaBH_4$ was decreased to 0.02 mL/s, we observed interesting nanostructures formed through connection of nanospheres one by one, looking like "pearl necklaces" (Figure 2b). We called these structures "nanonecklaces". The diameters of the nanonecklaces were in the range of 50−200 nm.

* To whom correspondence should be addressed. Tel/Fax: 86 27 6786 7535. E-mail: zhanglz@mail.ccnu.edu.cn.
[†] Central China Normal University.
[‡] Xuchang University.
[§] The Chinese University of Hong Kong.

10.1021/cg060633a CCC: $37.00
Published on Web 01/06/2007

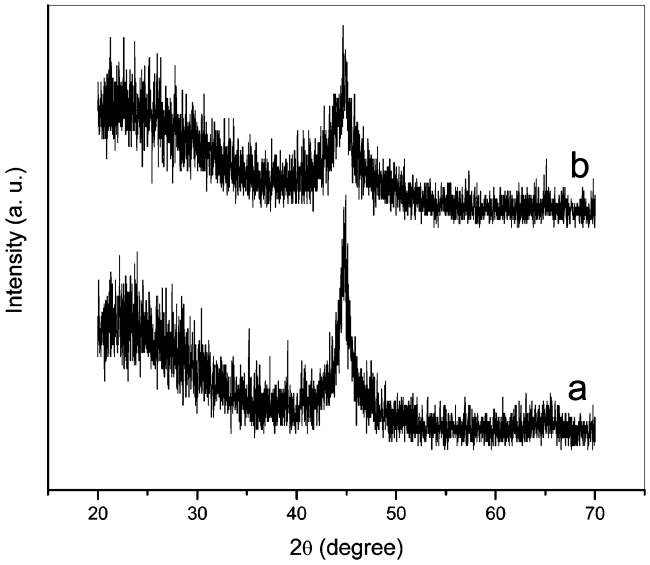

Figure 1. XRD patterns of the as-prepared samples obtained with different addition rates of $NaBH_4$ solution: (a) 0.5 and (b) 0.02 mL/s.

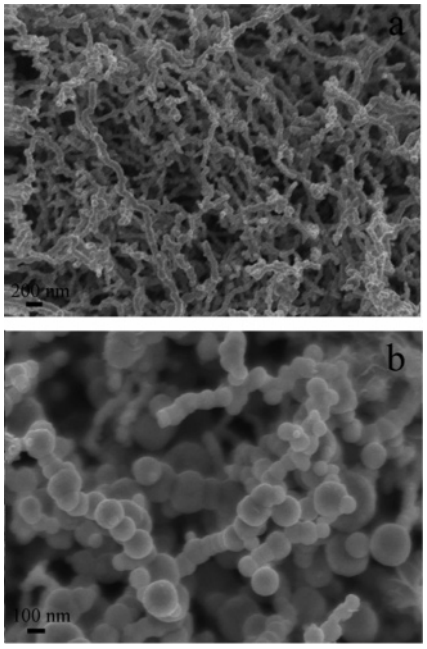

Figure 2. SEM images of the as-prepared samples obtained with different addition rates of $NaBH_4$ solution: (a) 0.5 and (b) 0.02 mL/s.

The resulting nanostructures were further investigated by transition electron microscopy (TEM). Figure 3 displays TEM images of the as-prepared nanostructures obtained under different conditions. The structures of nanowires and nanonecklaces were confirmed by the TEM images. Figure 3a shows a nanowire of about 50 nm in diameter. The nanowire was not straight, and its surface was also not smooth. Interestingly, the contrast between the gray edge and the dark center of the nanowire was easily observed, suggesting the core−shell structure of the nanowire. Figure 3b shows a nanonecklace, in which the diameters of the nanospheres were in the range of 100−150 nm. The contrast between the gray edge and the dark center of the nanospheres became more obvious, indicating the core−shell structure of the nanonecklaces.

The structures of core−shell nanowires and nanonecklaces were further investigated by high-resolution transition electron microscopy (HRTEM) and energy dispersive X-ray analysis (EDX) as well as elemental mappings. Figure 3 also shows HRTEM images of center and edge parts of a nanowire, a selective area electron diffraction of the nanowire, EDX, and elemental mappings of a nanowire. These results revealed that the nanowires were polycrystalline iron with an amorphous iron oxide sheath. The elemental mappings of Fe and O of a nanowire further confirmed the iron−iron oxide core−shell structure of the nanowire (Figure 3e−g). From Figure 3, we estimated the thickness of the oxide shell in the nanowires to be about 5−10 nm. Therefore, the diameters of metallic iron cores would be in the range of 30−40 nm because the total diameters of the nanowires were about 50 nm. Unfortunately, the nanonecklaces were unstable under e-beam irradiation. They melted fast when the e-beam was focused on the sample (Figure 4). This fact made it impossible to further analyze the nanonecklaces.

The chemical compositions of iron−iron oxide core−shell nanowires and nanonecklaces were further investigated by X-ray photoelectron spectroscopy (XPS). XPS survey spectra revealed that only elements Fe, O, and adventitious C existed in the nanowires and nanonecklaces (Figure 5). The further calculation of the peak area in Fe 2p and O 1s core level spectra gave an atom ratio of Fe and O elements of about 2:3, suggesting that the main component of the shell was Fe_2O_3. This result agreed with the TEM analysis. The Fe $2p_{3/2}$ and Fe $2p_{1/2}$ core levels appeared at the binding energies of 711.0 and 725.0 eV, respectively, consistent with the literature values of 710.9 and 724.6 eV for the bulk Fe_2O_3.[6] The shakeup peak at approximately 10 eV above the Fe $2p_{3/2}$ peak was further evidence of Fe^{3+}.[7] These data confirmed that the shells were Fe_2O_3. No signal of Fe_2O_3 in XRD patterns indicated that Fe_2O_3 shells of the nanowires and nanonecklaces were amorphous or that their sizes were too small to be detected by XRD. Besides the predominant peak at 710.9 eV and a shoulder at 724.6 eV being assigned to Fe in Fe_2O_3,[8] a peak at a low binding energy of 707.1 eV was observed in the spectrum of the nanonecklaces (Figure 5d). This peak was attributed to Fe $2p_{3/2}$ in pure iron. Because the XPS could only detect the photoelectrons from the outer surface of 10 nm, we thought that the thickness of the Fe_2O_3 shell in the nanonecklaces should be less than 10 nm because the metallic iron signal was detected. A higher binding energy shoulder was also fitted at about 713.7 eV, which may be attributed to an interaction between the Fe core and the Fe_2O_3 shell. The difference in Fe 2p core level spectra between the nanowires and the nanonecklaces indicated that the thickness of the Fe_2O_3 shell of the nanonecklaces was smaller than those of the nanowires. This illustrates that the instability and fast melting of the nanonecklaces during the HRTEM analysis may arise from the thinner protecting Fe_2O_3 shell and the lower melting point of nanosized Fe than that of Fe_2O_3 because of the smaller Fe crystal sizes in the nanonecklaces. Therefore, we conclude that both the resulting nanowires and the nanonecklaces are of Fe−Fe_2O_3 core−shell structures. According to TEM observation, the oxide shell of nanonecklaces in Figure 3b seems to be thicker than that of the nanowires in Figure 3a, which is opposite to the XPS conclusion. This difference is attributed to the fact that XPS gives statistical information of the samples but TEM provides observations of individual nanowires and nanonecklaces.

Magnetic properties of Fe−Fe_2O_3 core−shell nanowires and nanonecklaces were measured (Figure 6). The nanowires possessed a saturation magnetization (M_s) of 900 emu/g, while the nanonecklaces had a M_s value of merely 110 emu/g. The main reason for the low M_s of nanonecklaces was because of their smaller crystal sizes. The hysteresis loop of the nanowires

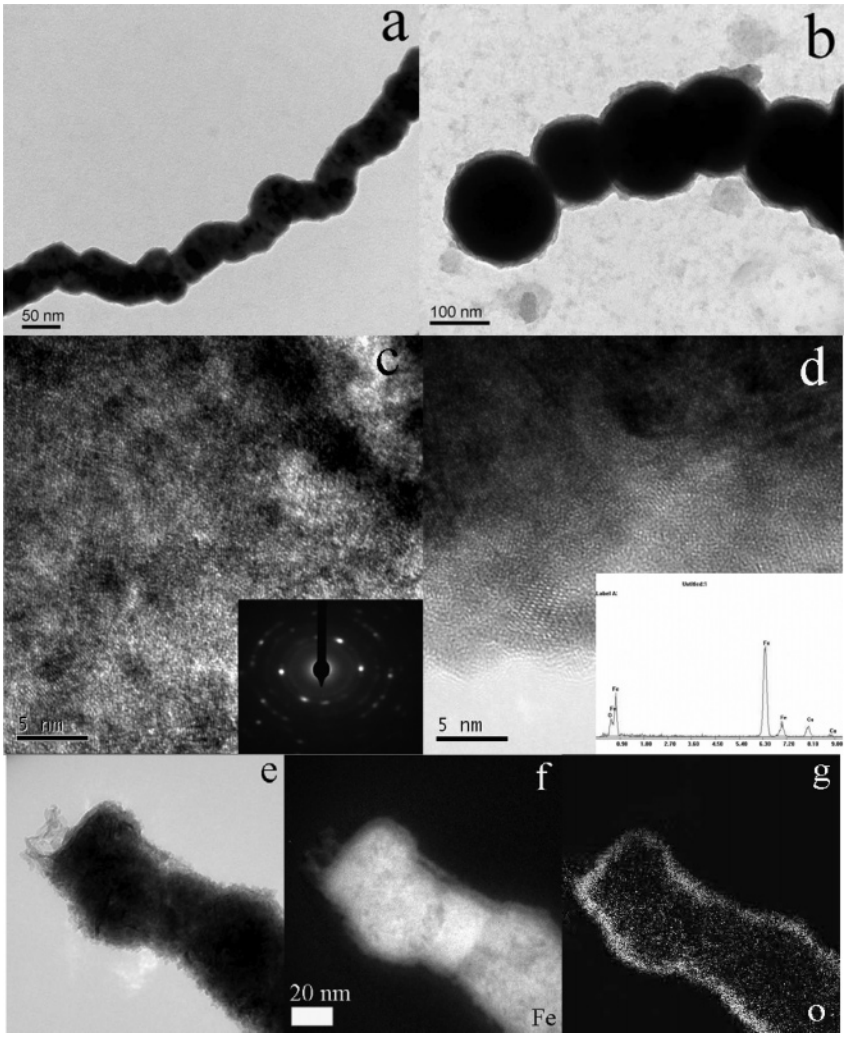

Figure 3. TEM images of the as-prepared nanostructures obtained with different addition rates of $NaBH_4$ solution: (a) 0.5 and (b) 0.02 mL/s. HRTEM images of center (c) and edge (d) parts of a nanowire, a selective area electron diffraction of the nanowire (inset of c), EDX (inset of d), and elemental mappings (e−g) of a nanowire.

displayed a coercivity (Hc) of about 0.62 kOe, which was slightly higher than that of the nanonecklaces (about 0.41 kOe), indicating the dependence of Hc over the thickness of the iron oxide shell and crystal size of iron core. The hysteresis loops showed smooth change of magnetization with applied field, suggesting that Fe core and Fe_2O_3 shell were in intimate contact and exchange coupled.[9]

The reduction of ferric solution by addition of $NaBH_4$ solution takes place as follows:[10]

$$Fe(H_2O)_6^{3+} + 3BH_4^- + 3H_2O = Fe^0\downarrow + 3B(OH)_3 + 10.5H_2\uparrow$$

For a typical reduction reaction of the above reaction, the electrochemical half-reaction and E^0 for ferric ion, H_2, and borohydride ion are given as follows:

$$Fe^{3+} + 3e^- \rightarrow Fe \quad E^0 = -0.036\ V$$

$$2H^+ + 2e^- \rightarrow H_2 \quad E^0 = 0.00\ V$$

$$B(OH)_3 + 7H^+ + 8e^- \rightarrow BH_4^- + 3H_2O \quad E^0 = -0.481\ V$$

Therefore, the reduction of iron by H_2 is not feasible or exceedingly difficult because of the more negative reduction

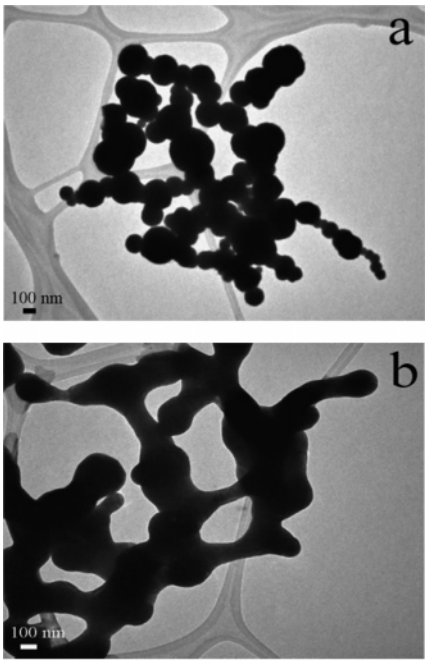

Figure 4. TEM images of the nanonecklaces before (a) and after (b) being focused by electron beam.

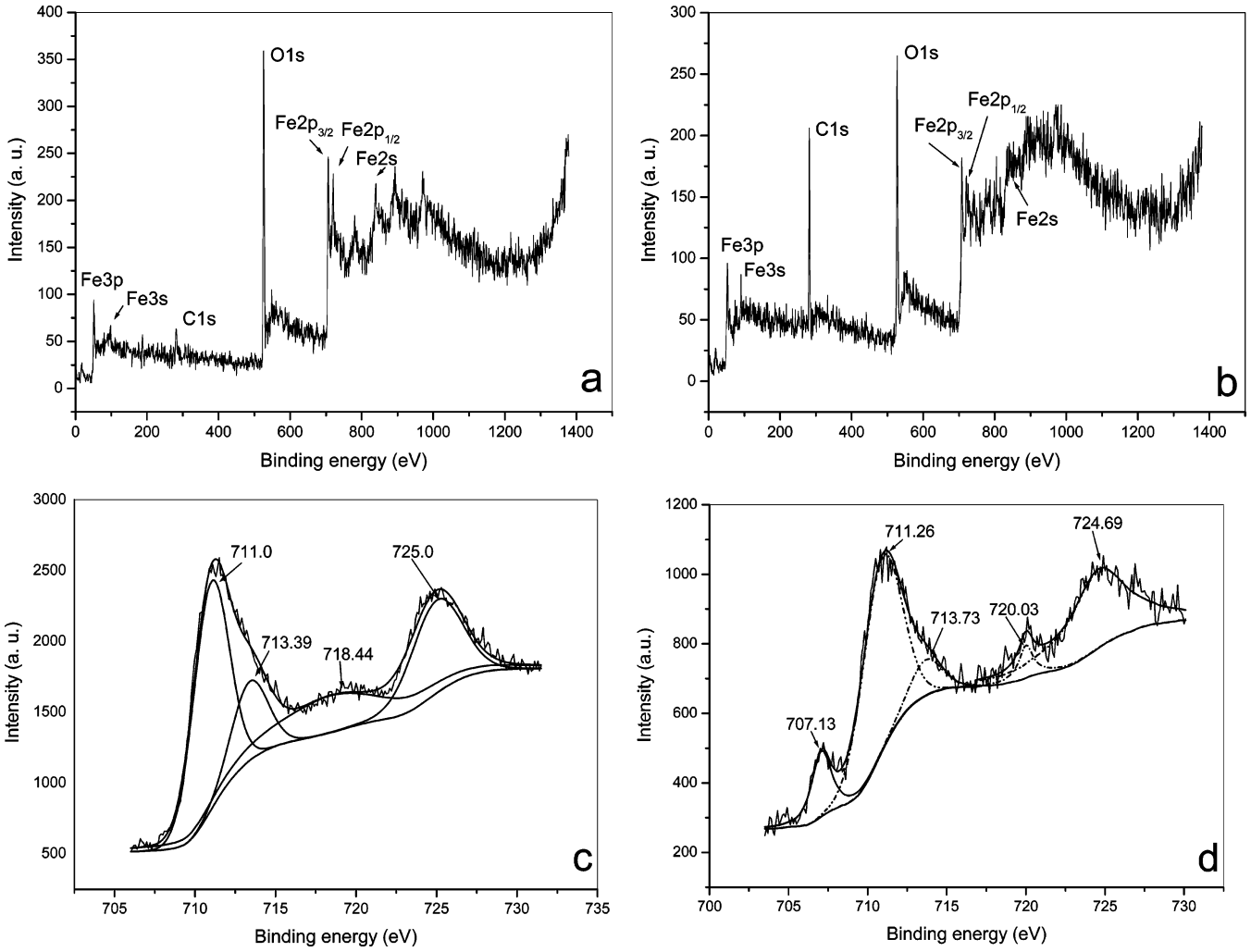

Figure 5. XPS profiles of the (a) survey spectrum of nanowires, (b) survey spectrum of nanonecklaces, (c) Fe 2p core level spectrum of the nanowires, and (d) Fe 2p core level spectrum of the nanonecklaces.

potential of Fe^{3+}/Fe than that of H^+/H_2. So, the reaction driving force arises from the large reduction potential gap between Fe^{3+}/Fe and $[B(OH)_3, H^+]/(BH_4^-, H_2O)$. The H_2 may prevent the freshly produced iron from oxidation during the reaction process.

On the basis of the above data, we proposed possible formation mechanisms of Fe−Fe_2O_3 core−shell nanowires and nanonecklaces as follows. As soon as $NaBH_4$ solution was added to ferric solution, Fe nuclei would produce under the protection of H_2 in situ formed. These nuclei would grow into nanospheres because the spherical shape has the lowest energy at equilibrium.[11] Meanwhile, self-assembly of nanospheres that were forming or had formed to more stable nanostructures would compete with the growth of nanospheres because of the magnetic property of Fe nanostructures. When the addition of $NaBH_4$ solution was fast, more Fe nuclei formed, resulting in larger magnetic interactions among Fe nuclei and/or the nanospheres that were forming or had formed. Therefore, the self-assembly process of Fe nuclei and renascent nanospheres would overwhelm the growth process of nanospheres, resulting in the formation of nanowires. This mechanism was proved by the existence of some spherical particles in the nanowires (Figure 3e). When the addition of $NaBH_4$ solution became slow, fewer Fe nuclei formed. Because of insufficient magnetic interaction, Fe nuclei would grow into well-defined nanospheres first. With the size and quantity increases of the crystals in the nanospheres, the magnetic interaction became stronger and stronger. Therefore, the formed nanospheres would subsequently assemble into nanonecklaces one by one, liking the fabrication of pearl necklaces (Figure 3b). Although the diameters of the nanonecklaces were larger than those of the nanowires, the crystal sizes of the primary particles in nanonecklaces were smaller than those in nanowires. This was because the faster addition of $NaBH_4$ solution produced more Fe nuclei, resulting in larger crystal sizes of the primary particles in nanowires. During the processes of drying, transportation, and storage, surface iron nanoparticles of the nanowires and the nanonecklaces were oxidized because of their high reactivity. This resulted in the final formation of Fe−Fe_2O_3 core−shell nanowires and nanonecklaces. We also performed experiments with other addition rates of $NaBH_4$ solution. When the addition rate was higher than 0.5 mL/s, Fe−Fe_2O_3 core−shell nanowires could also be obtained. However, the lengths of the resulting nanowires became shorter than those obtained at 0.5 mL/s. When the addition rate was between 0.5 and 0.02 mL/s, nanowires and nanonecklaces coexisted in the product. However, if the addition rate was lower than 0.02 mL/s, only separated nanospheres could be obtained. Kutty and co-workers found that the growth of cobalt ferrite shell/iron oxide core nanowires was through a mechanism of preferential growth of a particular crystal face.[12] However, it was difficult for us to find out the growth direction of the nanowires and nanonacklaces because of their polycrystalline nature.

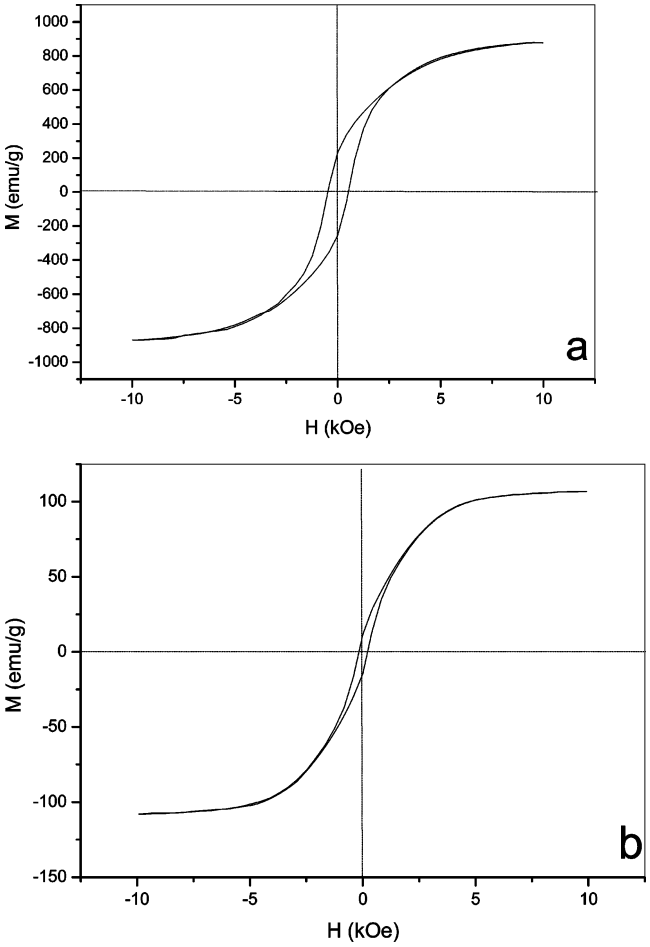

Figure 6. Magnetic hysteresis loops of the nanowires (a) and nanonecklaces (b).

Both core−shell Fe−Fe_2O_3 nanowires and nanonecklaces are very stable because of the protection of oxide shells. Their stabilities make it possible to apply them in environmental remedies. The Fenton reaction is one of the effective advanced oxidation processes (AOPs) for wastewater treatment, which is well-known as the production of hydroxyl radicals by reaction between Fe^{2+}/Fe^{3+} and H_2O_2.[13,14] However, the pH range for Fenton oxidation process efficiently work is very narrow (pH 2−3). Therefore, many efforts are being made to extend work pH ranges of Fenton reactions to neutral or base. In this study, we selectively used core−shell Fe−Fe_2O_3 nanowires as the Fenton iron reagent. We interestingly found that an electrochemical-assisted Fenton-like reaction system with the Fe−Fe_2O_3 core−shell nanowires as the iron source could much more efficiently degrade organic dye pollutants in water than that with Fe^{2+} ions under neutral pH (Figure 4a). Moreover, in ultrasound-assisted Fenton-like reaction systems to degrade organic dye pollutants in water under pH 2, Fe−Fe_2O_3 core−shell nanowires were also much more efficient than Fe^{2+} ions (Figure 7b). These preliminary results suggest that Fe−Fe_2O_3 core−shell nanostructures possess strong potential for environmental remedies, because these nanostructures cannot only extend the pH range for Fenton reaction and omit the pH adjustment process in classic Fenton reactions but also realize the recycling of iron sources and avoid the contamination caused by iron ions in classic Fenton reactions. More importantly, H_2O_2 was generated by an electrochemical reaction and ultrasound in these two systems. This would decrease the costs of the systems. Detailed

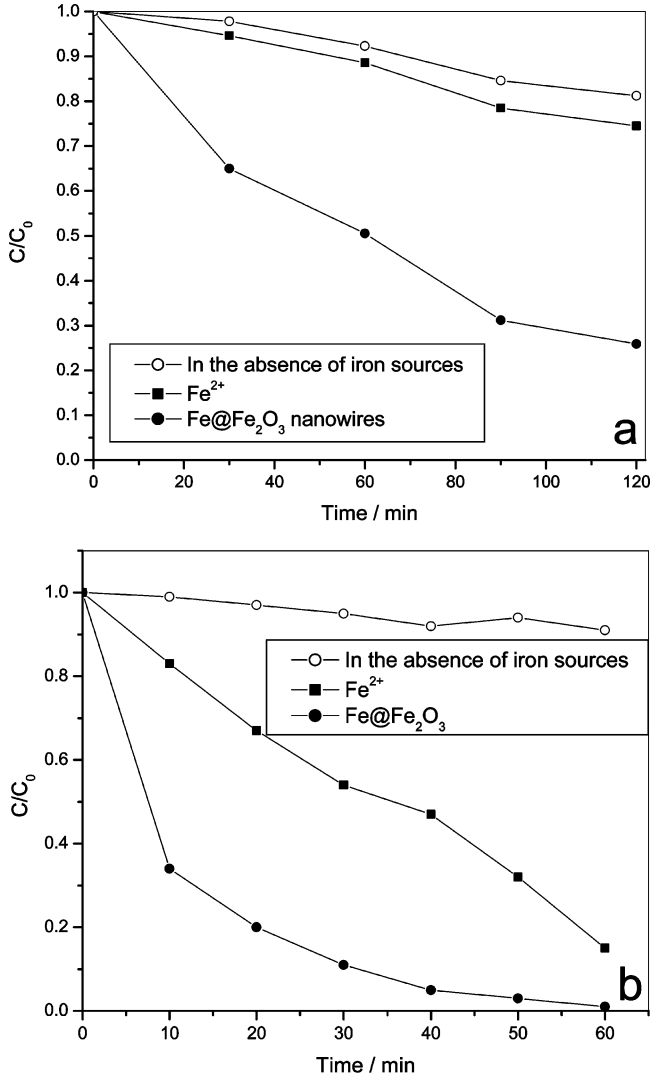

Figure 7. (a) Degradation of rhodamine B (RhB) by electrochemical-assisted Fenton-like processes with Fe−Fe_2O_3 nanowires and Fe^{2+} as iron sources, respectively. The initial concentration of RhB, 5 mg/L; pH 7; $E = 1.2$ V; the used amounts of Fe−Fe_2O_3 and Fe^{2+}, 1 mmol. (b) Degradation of RhB by ultrasound assisted Fenton-like processes with Fe−Fe_2O_3 and Fe^{2+} as iron sources, respectively. The initial concentration of RhB, 5 mg/L; pH 2; the used amounts of Fe−Fe_2O_3 and Fe^{2+}, 0.9 mmol.

studies are in progress to understand the degradation mechanism of RhB in the two Fenton-like systems using Fe−Fe_2O_3 core−shell nanowires as iron sources.

In summary, we reported a simple method to selectively synthesize Fe−Fe_2O_3 core−shell nanowires and nanonecklaces. These iron-containing nanostructures are promising materials in magnetic, environmental, and catalytic fields. Moreover, we have scaled up this method for production of samples in gram quantities.

Acknowledgment. The work described in this paper was partially supported by the National Science Foundation of China (Grants 20503009 and 20673041) and Open Fund of Key Laboratory of Catalysis and Materials Science of Hubei Province (Grants CHCL0508 and CHCL06012).

References

(1) Zeng, H.; Li, J.; Wang, Z. L.; Liu, J. P.; Sun, S. H. *Nano Lett.* **2004**, *4*, 187−190.

(2) Dumitrache, F.; Morjan, I.; Alexandrescu, R.; Ciupina, V.; Prodan, G.; Voicu, I.; Fleaca, C.; Albu, L.; Savoiu, M.; Sandu, I.; Popovici, E.; Soare, I. *Appl. Surf. Sci*. **2005**, *247*, 21−31.
(3) Bönnemann, H.; Brijoux, W.; Brinkmann, R.; Joussen, T. *Angew. Chem., Int. Ed. Engl.* **1990**, *29*, 273−275.
(4) Tsai, K. L.; Dye, J. L. *J. Am. Chem. Soc.* **1991**, *113*, 1650−1652.
(5) Carpenter, E. E.; Calvin, S.; Stroud, R. M.; Harris, V. G. *Chem. Mater*. **2003**, *15*, 3245−3246.
(6) Allen, G. C.; Curtis, M. T.; Hooper, A. J.; Tucker, P. M. *J. Chem. Soc. Dalton Trans.* **1974**, *14*, 1525−1527.
(7) Liang, R. Y.; Huang, N. K.; Zhang, H. L.; Yang, B.; Wang, D. Z. *Appl. Surf. Sci*. **1999**, *150*, 39−42.
(8) Mills, P.; Sullivan, J. L. *J. Phys. D Appl. Phys.* **1983**, *16*, 723−725.
(9) Zeng, H.; Li, J.; Wang, Z. L.; Liu, J. P.; Sun, S. *Nature* **2002**, *420*, 395−398.
(10) Glavee, G. N.; Klabunde, K. J.; Sorensen, C. M.; Hadjipanayis, G. C. *Inorg. Chem.* **1995**, *34*, 28−35.
(11) CuShing, B. L.; Kolesnichenko, V. L.; O'Connor, C. J. *Chem. Rev.* **2004**, *104*, 3893−3946.
(12) Sudakar, C.; Kutty, T. R. N. *J. Magn. Magn. Mater.* **2004**, *279*, 363−374.
(13) Casado, J.; Fornaguera, J.; Galan, M. I. *Environ. Sci. Technol.* **2005**, *39*, 1843−1847.
(14) Ma, J. H.; Song, W. J.; Chen, C. C.; Ma, W. H.; Zhao, J. C.; Tang, Y. L. *Environ. Sci. Technol*. **2005**, *39*, 5810−5815.

CG060633A